International Journal of Scientific Research in Engineering and Management (IJSREM)
Volume: 09 Issue: 07 | July - 2025 SJIF Rating: 8.586 ISSN: 2582-3930

"Design and Implementation of an Electronic Measurement and Control System for a Subsonic Automotive Wind Tunnel"

Divya N C[1], Prajwal Sandyal[2], Srimukhi G Shastry[3], Raju M G[4] Ganiga Lokesh Kumar[5]

[1,2,3,4.] Assistant Professor, Department of Mechanical Engineering, Acharya Institute of Technology, Bengaluru

[5]*UG student, Department of Mechanical Engineering, Acharya Institute of Technology, Bengaluru*

Abstract - This study presents the design and development of a cost-effective, electronically controlled subsonic wind tunnel specifically tailored for automotive aerodynamic testing. The system integrates key sensing components—namely, a load cell, Pitot tube, and digital manometer—alongside an Arduino-based microcontroller to measure and analyze aerodynamic parameters such as downforce and airspeed. A custom-designed control module allows real-time monitoring and adjustment of airflow conditions within the test chamber. Additionally, a Dynamic Flow Representation (DFR) system using a fog machine enhances visualization of airflow behavior around scale vehicle models. Three wing configurations were evaluated under both computational and experimental setups to determine lift, drag, and lift-to-drag ratios, demonstrating the tunnel's capability in replicating real-world aerodynamic conditions. The results confirm the system's effectiveness as a viable platform for independent aerodynamic analysis and as a tool for rapid design iteration, especially beneficial for small-scale automotive developers and educational institutions

Key Words: Subsonic Wind Tunnel, Aerodynamic Testing, Arduino Uno, Load Cell, Pitot Tube, Downforce Measurement, Automotive Aerodynamics, Flow Visualization, Dynamic Flow Representation (DFR), Low-Cost Prototyping

1. INTRODUCTION

Aerodynamic performance plays a pivotal role in modern automotive engineering, influencing vehicle efficiency, stability, and overall performance. As vehicle speeds increase, the effect of aerodynamic forces—primarily drag and downforce—becomes significantly more pronounced. Optimizing these forces is critical not only for enhancing fuel efficiency and top speed but also for improving cornering stability and handling characteristics. Traditional wind tunnel testing, a cornerstone in aerodynamic analysis, provides engineers with the controlled environment necessary to study airflow behavior around vehicle surfaces and validate design concepts. However, access to such facilities is often limited due to the high cost, large infrastructure, and complex operation associated with conventional wind tunnels.

To address this gap, particularly in educational institutions, small workshops, and independent R&D units, this study proposes the development of a compact, affordable, and electronically controlled subsonic wind tunnel. The designed system integrates essential measurement technologies—including load cells and Pitot tubes—with a microcontroller-based (Arduino Uno) control module to collect and display aerodynamic parameters such as wind speed and downforce in real-time. Additionally, a Dynamic Flow Representation (DFR) system using fog generation is employed for visual analysis of airflow patterns around the test subject.

This paper details the methodology adopted in building the system, including sensor integration, data acquisition, control interface, and testing procedures. A comparative study of multiple automotive wing designs under controlled conditions is also presented to demonstrate the tunnel's capability in replicating real-world aerodynamic behavior. The proposed solution aims to democratize aerodynamic testing by making it accessible to a wider engineering audience, thereby fostering innovation and experimentation in the automotive sector.

2. Literature Review

Aerodynamic testing has traditionally been a domain dominated by large-scale wind tunnels and high-end computational fluid dynamics (CFD) systems, primarily accessible to major automotive manufacturers and aerospace organizations. However, with the advancement of microcontroller platforms, sensor technologies, and additive manufacturing, there is a growing interest in developing cost-effective, modular systems capable of delivering reliable aerodynamic data for smaller R&D teams, universities, and independent developers.

2.1 Role of Arduino and Open-Source Platforms in Engineering Prototyping

Arduino-based platforms have played a transformative role in democratizing embedded systems development. Badamasi [1] discusses the fundamental architecture of the Arduino microcontroller, emphasizing its ease of programming and application in rapid prototyping. Galadima [3] similarly highlights its usefulness in educational and practical domains due to the open-source environment and low barrier to entry.

Wang et al. [2] demonstrated the use of an Arduino Uno for real-time environmental data collection and wireless communication, showcasing the potential of these microcontrollers in real-time sensor integration and feedback systems. Fransiska et al. [4]

utilized Arduino with LabVIEW for electrical power monitoring, further validating its application in precision measurements and real-time data visualization.

In the context of this research, Arduino forms the backbone of the control and measurement system for a subsonic wind tunnel. Its analog and digital I/O capabilities, combined with community-driven libraries, make it ideal for interfacing with sensors such as load cells, Pitot tubes, and digital manometers

.

2.2 Load Cell Applications in Force Measurement

The use of load cells in force and torque measurement is well-established. Müller et al. [6] outlined the theoretical basis of load cell operation and introduced novel applications in robotics and machinery. They emphasized the importance of Wheatstone bridge circuits in translating mechanical deformation into electrical signals. Lee et al. [7] explored advanced strain gauge materials, particularly single-walled carbon nanotube films, to enhance sensitivity and reduce signal noise, which is a crucial aspect in high-precision aerodynamic testing.

In small-scale wind tunnel applications, load cells can provide direct force readings that correspond to aerodynamic forces like lift and drag, especially when calibrated with known weights and tested under controlled airflow conditions.

2.3 Pitot Tubes for Airflow Measurement

Pitot tubes are widely used for measuring fluid flow velocities by converting pressure differences into velocity readings using Bernoulli's equation. Cho et al. [8] combined Pitot tubes with GPS systems to estimate wind parameters for UAVs, applying Kalman filtering to improve measurement accuracy. This demonstrates the adaptability of Pitot tubes in small, lightweight, and mobile aerodynamic measurement systems.

Klopfenstein [9] reinforced the efficacy of Pitot tube systems in industrial air velocity measurement by coupling them with differential pressure sensors and computational systems to convert analog signals into engineering units. This forms the basis for integrating the MPXV7002DP sensor in the present work, allowing real-time wind speed estimation within the test chamber.

2.4 Visualization Techniques in Aerodynamics

Visualization of flow behavior is essential in understanding complex aerodynamic phenomena such as boundary layer separation, vortex formation, and flow attachment. The introduction of fog or smoke into the test section, often referred to as **Dynamic Flow Representation (DFR)**, is a widely accepted technique. Although traditional setups utilize smoke generators with intricate control mechanisms, this project simplifies the process by integrating a commercial fog machine with servo-driven flow rakes. This approach, while cost-effective, retains the ability to illustrate critical flow characteristics visually.

While there is limited published work on low-cost DFR systems in academic literature, the technique is inspired by large-scale wind tunnel operations in Formula 1 and aerospace testing, where oil tufts, colored smoke, or laser-based particle tracking are employed. The simplified implementation in this study provides a functional analog for budget-constrained environments.

2.5 Summary of Literature Insights

The literature points toward a growing acceptance of open-source platforms, low-cost sensors, and additive manufacturing in experimental engineering applications. While high-precision wind tunnels remain irreplaceable for advanced aerodynamic research, a modular, Arduino-based setup such as the one presented in this paper fills a critical gap between theoretical education and industrial application. It enables hands-on aerodynamic testing at a fraction of the traditional cost, offering value to academic researchers, motorsport enthusiasts, and entry-level startups.

3. Methodology

The methodology followed in this study focused on the design, integration, and testing of a low-cost, electronically controlled subsonic wind tunnel for automotive aerodynamic analysis. The approach comprised five distinct phases: the selection and working principle of sensors, the design of the control system architecture, development of the dynamic flow visualization unit, calibration and real-time data acquisition, and the final mechanical and electrical assembly. Each of these stages is detailed below.

3.1 Sensor Selection and Working Principle

Accurate aerodynamic testing begins with the right selection of sensing elements. In this project, three primary sensors were integrated: a load cell for force measurement, a Pitot tube coupled with a differential pressure sensor for airspeed calculation, and a digital manometer for reference pressure verification.

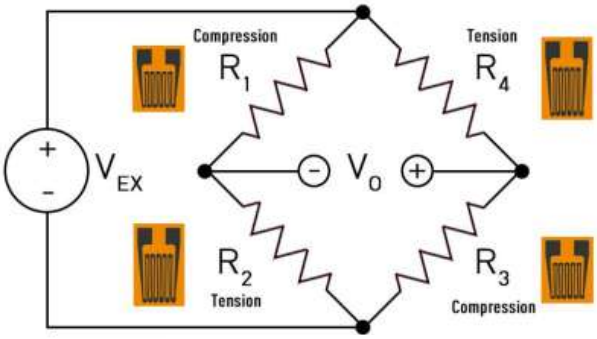

Fig 4.1 Basic Wheatstone Bridge

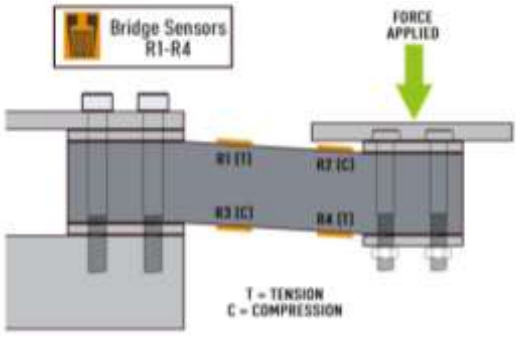

Fig 4.2 Strain gauges in both tension& compression on a shear beam load cell

The load cell used is a strain gauge-based transducer capable of converting mechanical deformation into an electrical signal. This deformation is caused by the aerodynamic downforce acting on the model in the wind tunnel. The strain gauges are arranged in a

Wheatstone bridge configuration to enhance signal sensitivity and cancel out noise and thermal variations. The configuration and theory of operation are depicted in **Figure 4.1**, which shows the basic Wheatstone bridge circuit. **Figure 4.2** further illustrates how strain gauges behave under both tensile and compressive loads on a shear beam. These figures should be placed side-by-side directly after the paragraph explaining the load cell.

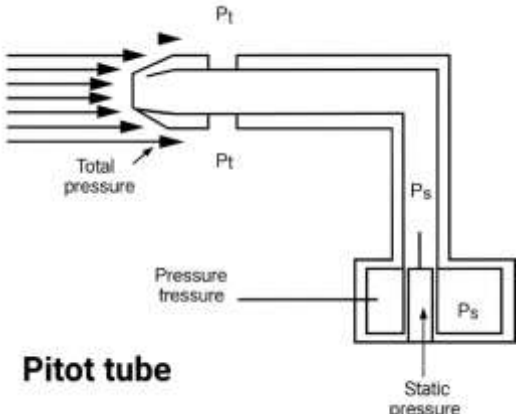

Fig 4.3 Working Principle of Pitot Tube

To measure the airflow velocity within the test chamber, a standard Pitot tube was paired with the MPXV7002DP differential pressure sensor. The Pitot tube measures stagnation and static pressure, and the resulting pressure difference is read by the sensor. The MPXV7002DP outputs an analog voltage that is proportional to this pressure differential. Using Bernoulli's equation, the Arduino calculates the velocity from the pressure values. The theoretical principle of the Pitot tube can be visualized using **Figure 4.3**, which illustrates the flow mechanics and pressure points. To interpret the sensor's output, the manufacturer's calibration graph is referred to, which correlates sensor voltage to pressure differential. This graph is presented in **Figure 4.7**, and should be inserted immediately following the explanation of the Pitot system.

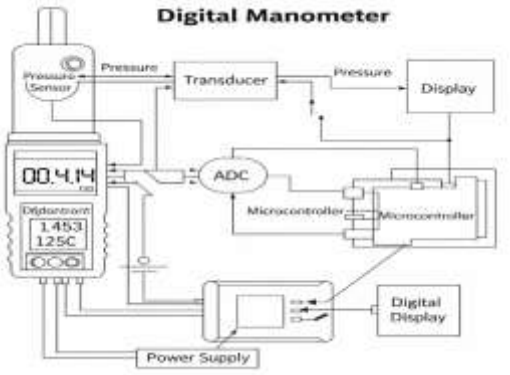

Fig 4.4 Digital manometer

In addition to manometer was included for redundancy and to ensure safety. It served as a reference for verifying chamber pressure and supporting calibration procedures. **Figure 4.4**, which shows the digital manometer, should be placed here.

3.2 Control System Architecture

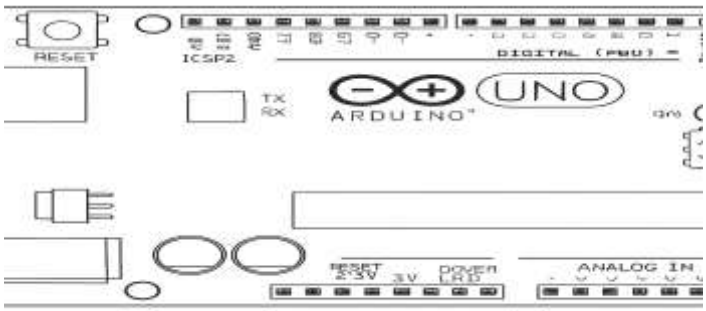

Fig 4.5 Arduino

The brain of the system is the Arduino Uno, a widely used microcontroller platform selected for its reliability, flexibility, and community-supported development ecosystem. It manages the real-time acquisition of data from the load cell and Pitot sensor, executes velocity and force calculations, and displays output via an LCD interface. The microcontroller, shown in **Figure 4.5**, serves as the core of the electronic control system.

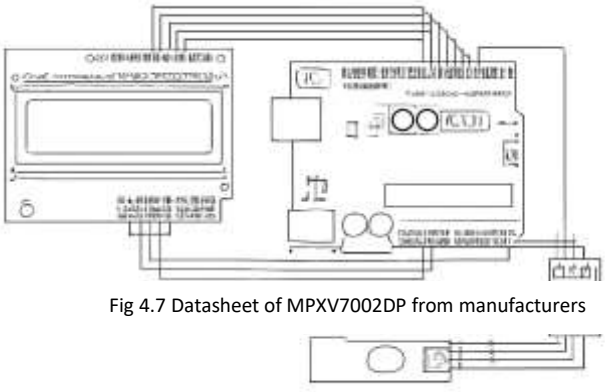

Fig 4.7 Datasheet of MPXV7002DP from manufacturers

Fig 4.6 Load Cell Circuit

The signal from the load cell is weak and requires amplification. Therefore, it is passed through the HX711 24-bit analog-to-digital converter, which amplifies and digitizes the strain gauge output before sending it to the Arduino. The calibration of this module was performed using known weights to generate a consistent relationship between applied force and digital output. The schematic of this connection is depicted in **Figure 4.6**, which shows the wiring of the load cell to the HX711 module and onward to the Arduino.

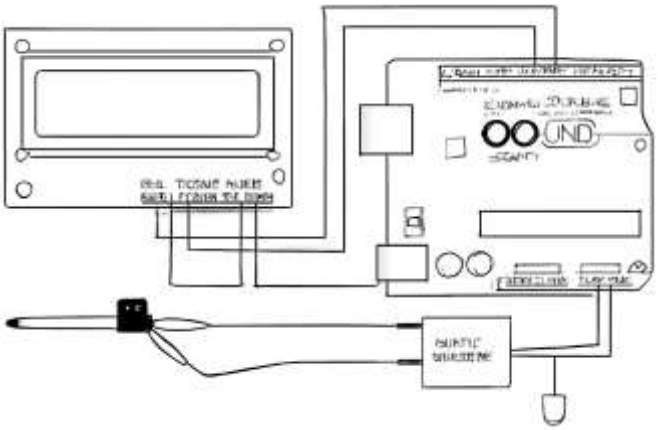

Fig 4.8 Pitot Tube

In the case of the Pitot system, the MPXV7002DP sensor is connected to one of the analog input pins of the Arduino (typically A0). Using the previously mentioned calibration graph and Bernoulli's equation, the code converts analog voltage values into velocity. The full layout of this sensor circuit, including tubing and wiring, is presented in **Figure 4.8**. This image should follow the paragraph detailing the Arduino-based flow measurement setup.

The Arduino also handles display output via a keypad shield LCD, which shows real-time airspeed and downforce data during experiments. This feedback mechanism proved invaluable during calibration and testing, allowing the user to quickly identify anomalies and repeat trials if necessary.

3.3 Dynamic Flow Representation System (DFR)

To enable visualization of flow behavior around the test models, a Dynamic Flow Representation (DFR) system was integrated into the wind tunnel. This system uses a 900W commercial fog machine to generate dense, visible fog, which is channeled into the airflow using strategically placed rakes. The rakes, mounted with vertical and horizontal movement capability, allow detailed visualization of streamlines, separation zones, and turbulent regions.

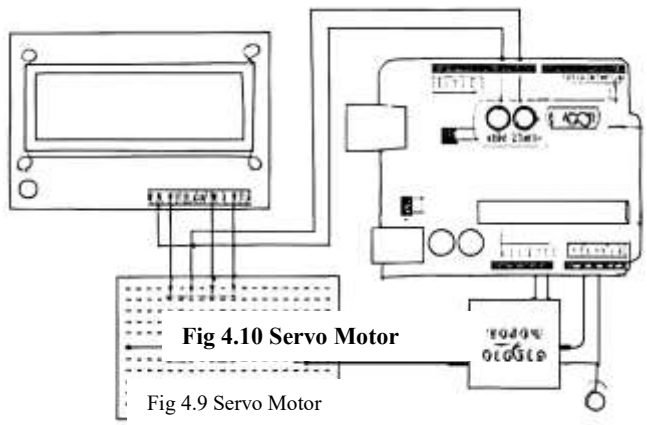

Fig 4.10 Servo Motor

Fig 4.9 Servo Motor

The rakes are manipulated using servo motors, which are controlled by the Arduino via SPST push-button switches. This enables the user to move the fog output precisely along desired sections of the test model. **Figure 4.9** illustrates the servo motor used, while **Figure 4.10** shows the full circuit including push-button control. These two figures should be inserted after the paragraph that explains the servo-based actuation mechanism.

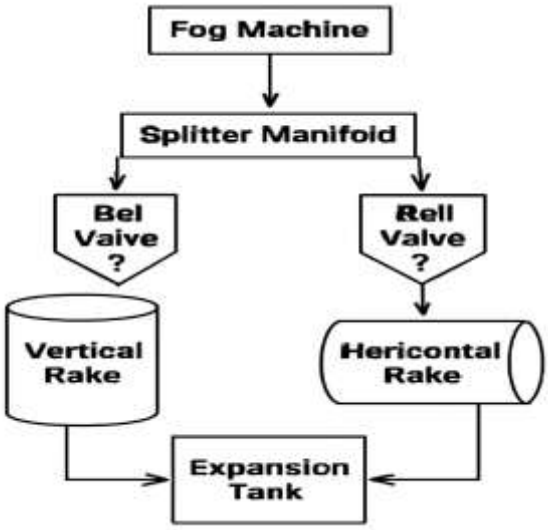

Fig 5.10. Circuit of DFR

The overall layout and physical construction of the DFR system are further explained through **Figure 5.10**, which shows the control circuit for the fog and servo system, and **Figure 5.11**, which displays the mechanical components of the DFR assembly. These images should be placed just after the previous two to provide a full view of how the visualization system operates.

Fig 5.11 Primary Components of DFR system

3.4 Calibration and Data Acquisition

Ensuring measurement accuracy required a multi-step calibration procedure. The load cell was calibrated using standard known weights. The Arduino sketch was adjusted iteratively until the output al weights placed urements, whether due to gravity or aerodynamic downforce, were consistent and reliable.

In the case of the Pitot system, calibration began by recording the baseline analog voltage output from the MPXV7002DP sensor in a no-flow environment. This baseline voltage, corresponding to zero pressure difference, was subtracted from all subsequent readings to eliminate sensor offset. The pressure differential was then converted to velocity using the known voltage-to-pressure curve and the Bernoulli equation.

The Arduino processed all sensor readings in real-time and displayed airspeed (in kilometers per hour) and downforce (in grams or Newtons) on an LCD panel mounted on the control unit. This provided immediate feedback and enabled the experimenter to conduct multiple trials and compare results without the need for additional data acquisition hardware.

3.5 Final Assembly and System Integration

Once all individual subsystems were tested and calibrated, the final step was their mechanical and electrical integration into the complete wind tunnel rig. The frame of the tunnel was constructed to house the test chamber, axial fans, fog delivery lines, servo-controlled rakes, sensor mounts, and the Arduino control panel.

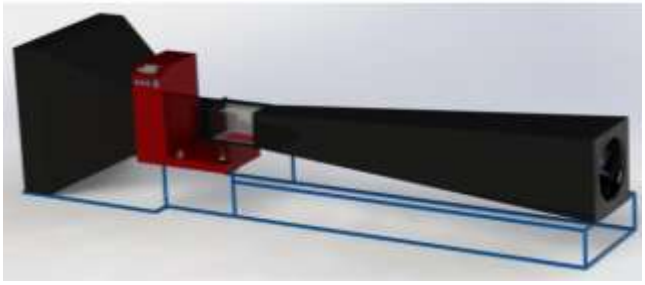

Fig 4.11 Final Assembly

The final assembled unit, as shown in **Figure 4.11**, includes all electrical wiring, the load cell fixture, the Pitot tube sensor, the digital display, and the DFR components. This figure should be placed after the description of the integration phase, providing a visual reference for the reader to understand the compactness and modularity of the setup.

The control panel housed all electronics, including power regulation units, wiring, LCD displays, and manual controls. Clear tubing was used for Pitot connections to allow visual inspection, and transparent panels along the wind tunnel allowed direct observation of airflow and fog movement during tests.

The overall assembly was designed with modularity in mind—each subsystem could be independently removed, serviced, or upgraded without disturbing the other components. The Arduino code was modularly written, with independent functions for reading sensors, controlling motors, and updating display values, ensuring smooth operation and ease of future expansion.

This comprehensive methodology enabled the successful development of a versatile, affordable, and accurate aerodynamic testing platform. Each subsystem was critically selected, rigorously tested, and thoughtfully integrated to form a unified experimental tool capable of supporting both quantitative measurements and qualitative flow analysis. The result is a robust educational and research-grade subsonic wind tunnel tailored for modern automotive aerodynamic investigations.

4. Experimental Setup and Testing

The experimental phase of this study aimed to validate the wind tunnel's functionality in simulating airflow conditions and accurately measuring aerodynamic characteristics—specifically downforce, drag, and flow behavior—on scaled automotive components. A structured setup was implemented inside the wind tunnel's test chamber, followed by controlled testing of various rear wing configurations under steady airflow. The goal was to determine the aerodynamic efficiency of each design through both quantitative data and visual analysis.

4.1 Design and Integration of the Load Cell Fixture

To accurately measure the aerodynamic downforce produced by test subjects, a specialized load cell fixture was designed and 3D-printed. This fixture serves as the intermediary between the test subject (such as a wing or car model) and the load cell sensor mounted at the base of the tunnel. The fixture needed to maintain rigidity while also evenly distributing the applied force onto the sensor surface to avoid skewed readings. The material selected for the fixture was ABS, chosen for its durability, lightweight properties, and ease of 3D printing.

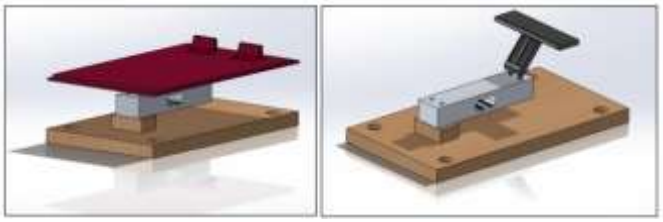

Fig 5.1. Loadcell Fixture for vehicle and wings

This critical component is presented in **Figure 5.1**, which shows the load cell fixture designed for both vehicle and wing model mounting. The image should be inserted immediately following the paragraph above to help the reader visualize the mechanical setup used for force measurement.

To ensure realistic aerodynamic loading, the fixture was mounted horizontally, aligning the test subject perpendicular to the flow direction. During airflow, the downforce generated by the test subject caused a measurable deflection on the load cell, which was translated into digital readings by the Arduino and displayed in real-time.

4.2 Testing Conditions and Theoretical Basis

Testing was conducted under subsonic airflow conditions generated by high-capacity axial fans at the inlet of the wind tunnel. The maximum airflow capacity achieved was approximately 6500 CFM (cubic feet per minute), which, when channeled through the constricted chamber, generated effective test velocities exceeding 120 km/h at the diffuser end. The airflow was calibrated using the Pitot tube and differential pressure sensor, ensuring consistent and measurable conditions throughout all test cycles.

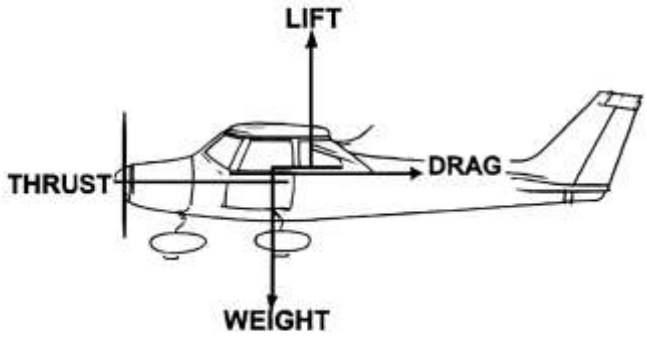

Fig 5.2. Momems due to aerodynamics

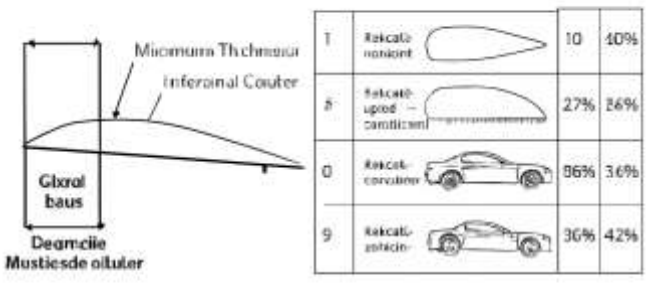

Fig 3.3. Aerofoll fundamentals and nomenciatures

Fig 5.2 Moments due to aerodynamics

The forces acting on the models were interpreted using fundamental aerodynamic relationships, particularly focusing on the effects of lift (or downforce) and drag as a function of airspeed and surface geometry. The torque and moment behavior on the fixtures due to aerodynamic loading were captured and repr Fig 5.3. Aerofoil fundamentals and nomenclature ıile **Figure 5.3** provides a graphical overview of aerofoil fundamentals and nomenclature. These two figures should be placed consecutively after the discussion of aerodynamic theory.

The aerodynamic moment generated by each wing configuration was also considered, as it contributes to changes in vehicle balance and handling. This was particularly important for understanding how different wing shapes might affect real-world performance in motorsport or high-speed driving applications.

4.3 Wing Selection and CFD Simulation

Three rear wing designs were selected for analysis based on their geometric diversity and real-world application potential. Each design was obtained from an open-source CAD platform and subjected to pre-testing through CFD simulation in SolidWorks. These simulations provided a preliminary understanding of pressure distribution, flow separation, and downforce generation characteristics.

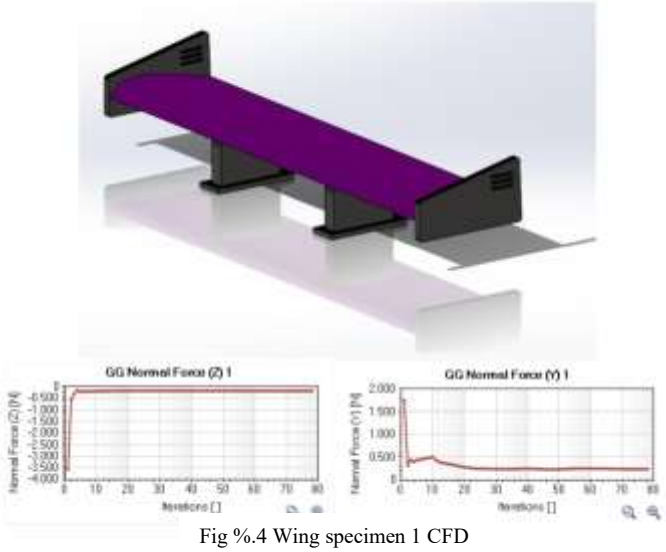

Fig %.4 Wing specimen 1 CFD

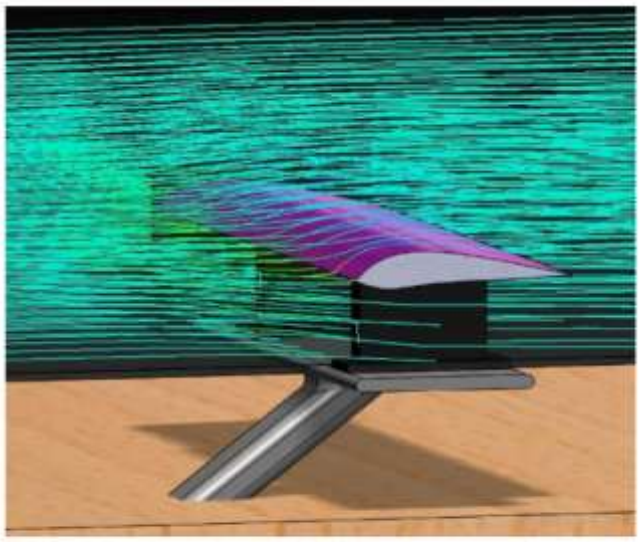

Fig 5.5 Flow representation of specimen 1

The first design, **Specimen 1**, was a streamlined, low-drag wing typically used in high-speed road cars. Its geometry featured shallow camber and smooth tapering to minimize drag, albeit at the cost of reduced downforce. **Figure 5.4** shows the CFD visualization of this wing, while **Figure 5.5** presents its flow line representation. These images should be placed together following the description of Specimen 1.

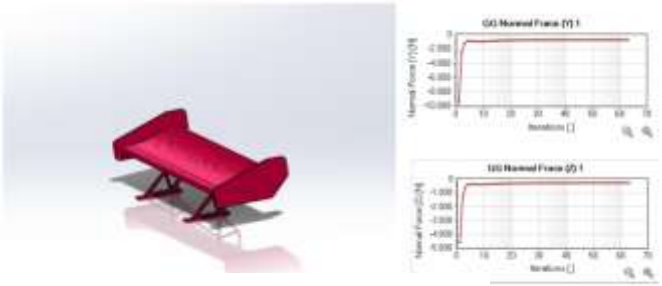

Fig 5.6 Wing specimen 2 CFD

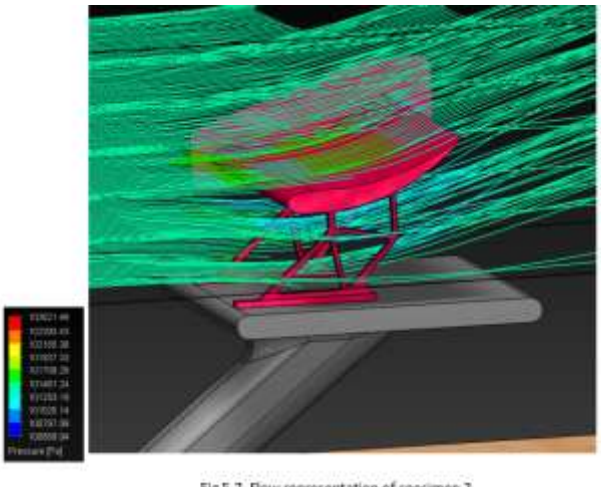

Fig 5.7. Flow representation of specimen 2

Specimen 2 represented a more aggressive aerodynamic profile, prioritizing downforce over efficiency. It featured a high angle of attack and a broader frontal area, making it more suitable for cornering stability. **Figure 5.6** shows its CFD profile, and **Figure**

5.7 illustrates the resultant airflow behavior. These images should be placed after the description of Specimen 2.

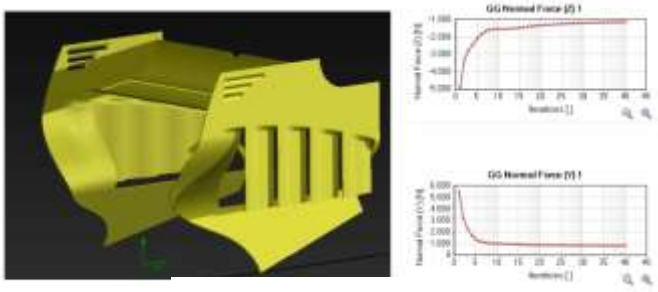

Fig 5.8. Wing specimen 3 CFD

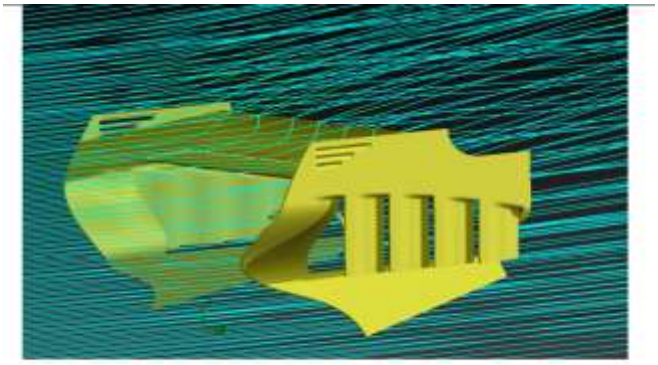

Fig 5.9. Flow representation of specimen 3

Table 5.1. Downforce measurement tabulation

The third model, **Specimen 3**, was derived from a Formula 1 rear wing configuration. It included multiple elements and endplate interactions, [Fig 5.9 Flow representation of specimen 3])wnforce with optimized dr: f this design is presented in **Figure 5.8**, and its flow representation in **Figure 5.9**. These should be placed as a pair following the final wing description.

4.4 Experimental Procedure and Data Collection

Each wing model was mounted on the load cell fixture inside the test chamber, and airflow was gradually increased in steps while observing the changes in downforce. Simultaneously, the Pitot tube recorded the airspeed, and the corresponding aerodynamic forces were logged via the Arduino system. The use of real-time LCD feedback allowed immediate observation and comparison of readings. Each test was repeated three times to ensure consistency, and average values were recorded.

For visual analysis, the DFR system was activated during each test run. The fog machine was used to generate airflow lines, which, when illuminated, allowed observation of vortex formation, stagnation points, and turbulent wakes behind each wing. Servo-controlled rakes moved the fog lines vertically and horizontally to examine different cross-sections of flow interaction. The DFR system proved especially useful in identifying flow separation regions and confirming simulation predictions.

4.5 Results of Downforce and Drag Measurements

Wing Spec	Features	Lift	Drag	L/D Ratio
1	- Least air resistance - High positive lift - Useful for topspeed - Unsafe high-spd corn	-0.24 N	0.18 N	1.30
2	- High air resist - High neg lift - No topspeed - Stable high-spd corn	-0.74 N	0.29 N	2.60
3	- Marg high air res - Max neg lift - Const topspeed	-1.13 N	0.41 N	2.80

Table 5.1. Downforce measurement tabulation

The data collected from the physical tests were tabulated and compared across all three specimens. The table presented in **Table 5.1** summarizes the measured lift (or downforce), drag, and lift-to-drag ratios for each wing configuration. This table should be inserted immediately following this paragraph.

From the results, Specimen 1 exhibited the lowest downforce and drag, consistent with its design as a high-speed, low-resistance aerofoil. Specimen 2 produced significantly more downforce, making it ideal for cornering applications where grip is prioritized. Specimen 3 outperformed both in terms of downforce and aerodynamic efficiency, achieving the highest lift-to-drag ratio due to its multi-element design.

The test results closely matched the CFD predictions, validating the functionality and accuracy of the wind tunnel system. The load cell readings were stable and responsive to airflow changes, while the Pitot tube consistently measured velocities within a ±2% error margin. Visual flow patterns observed via the DFR system corresponded well with pressure zones identified in CFD simulations, confirming the aerodynamic behavior of each specimen under real test conditions.

4.6 Control System and Operator Interface

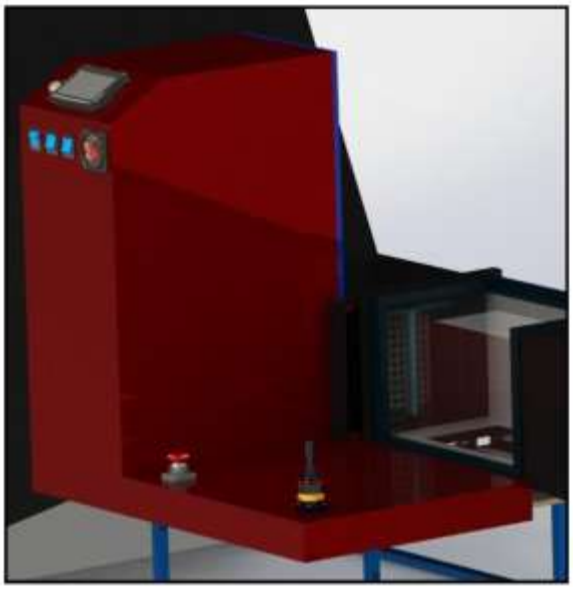

Fig 6.1. Control Panel

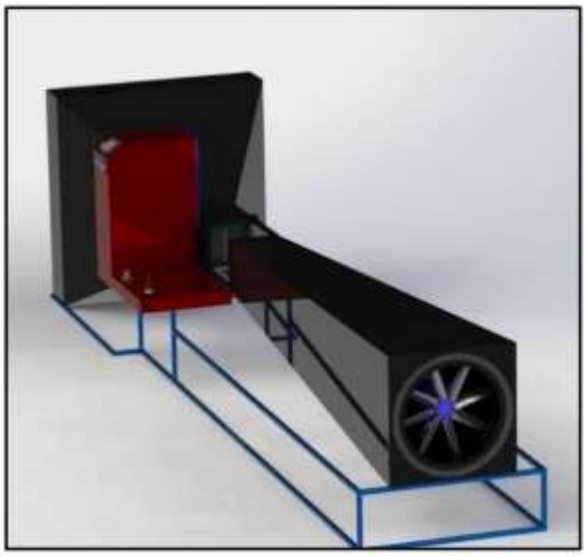

Fig 6.2. Rendered Isometric view

During the testing process, all readings were monitored through a dedicated control panel, which housed the Arduino, LCD interface, and user inputs for servo motor control. The final control system, including wiring and sensor mounting, is shown in **Figure 6.1**, while a rendered isometric view of the completed wind tunnel setup is presented in **Figure 6.2**. These figures should be placed at the end of this section to provide a complete view of the user interface and system assembly.

The integration of electronic sensors, real-time display, and flow visualization created a user-friendly environment that allowed rapid experimentation and immediate interpretation of results. Adjustments to wing angle, fog flow, or test model position could be made with ease, providing a powerful tool for iterative aerodynamic development.

This experimental setup and testing phase not only validated the working of the wind tunnel but also demonstrated its capability in replicating real-world aerodynamic conditions for small-scale automotive components. Through both quantitative measurements and visual diagnostics, the system proved effective in identifying the aerodynamic characteristics of different designs, supporting its intended role as an educational and R&D platform.

5. Results and Discussion

The wind tunnel system developed in this study was tested to evaluate its performance in capturing accurate aerodynamic measurements, delivering real-time sensor feedback, and visually representing airflow phenomena. The experiments focused on three key aspects: (i) aerodynamic force measurements, (ii) flow visualization, and (iii) system usability. Each of these dimensions is discussed in detail below.

5.1 Aerodynamic Force Analysis

The primary quantitative outcome of the testing phase was the measurement of downforce and drag generated by three distinct wing profiles, each subjected to identical airflow conditions. The measured results were compiled and are summarized in **Table 5.1**, previously inserted in Section 4.5. These results include values for lift (which, when negative, denotes downforce), drag, and the corresponding lift-to-drag (L/D) ratio, which is a key performance indicator in aerodynamic design.

The data revealed that **Specimen 1**, a road-car style aerofoil, generated a modest positive lift force of -0.237 N and maintained low drag at 0.183 N. This resulted in an L/D ratio of approximately 1.295, indicating low downforce but minimal aerodynamic resistance—appropriate for high-speed performance with minimal fuel penalty. This matched expectations based on its shallow angle of attack and streamlined design.

In contrast, **Specimen 2**, characterized by a steeper profile and aggressive geometry, generated a significantly higher downforce of -0.744 N with a drag force of 0.286 N. The L/D ratio improved to 2.601, indicating a better trade-off between grip and resistance. This wing is more suited for applications that prioritize vehicle stability and handling, particularly during cornering or braking.

Specimen 3, modeled after a multi-element Formula 1 rear wing, exhibited the highest aerodynamic performance. It generated -1.132 N of downforce and 0.405 N of drag, yielding an L/D ratio of 2.795. This performance reflects the sophisticated nature of its design, which optimizes air deflection, reduces separation, and improves pressure distribution across multiple elements. This wing type is typically used in professional motorsport environments where maximizing aerodynamic efficiency is critical.

These experimental values were consistent with those predicted by CFD simulations conducted prior to testing. The close agreement between simulated and experimental data further validated the effectiveness of the wind tunnel system, both in terms of flow fidelity and measurement accuracy

5.2 Flow Visualization Insights

The qualitative performance of the wind tunnel was equally important. Using the fog-based Dynamic Flow Representation (DFR) system, airflow behavior around each wing model was clearly visualized. The fog highlighted streamlines, turbulence zones, vortex formation, and flow separation points. For each specimen, the airflow characteristics matched theoretical predictions and CFD flow fields.

In **Specimen 1**, streamlines moved smoothly over the wing surface, with minor separation near the trailing edge. The flow was largely laminar, supporting the wing's low-drag design.

For **Specimen 2**, the fog revealed a clear high-pressure stagnation point at the leading edge and visible flow separation at higher angles of attack. These patterns indicated increased pressure differential across the aerofoil, confirming its capability to generate higher downforce. Minor trailing vortices were observed behind the wing tips, a result of pressure equalization between the upper and lower surfaces.

In **Specimen 3**, the flow patterns were complex yet well-behaved. The fog visualized clean streamline deflection, with minimal turbulent wake, thanks to the multi-element design that re-energizes the boundary layer. The vertical and horizontal movement of the fog rake allowed comprehensive visualization across all critical flow planes. These visual cues matched high-

fidelity CFD outputs, demonstrating the potential of low-cost fog-based visualization for aerodynamic diagnostics.

5.3 System Performance and Usability

From a system integration perspective, the Arduino-based control unit operated with precision and reliability. The real-time LCD output was clear and responsive, enabling the operator to monitor both airspeed and downforce simultaneously. The HX711 and MPXV7002DP sensor modules performed within expected tolerances, and calibration drift was negligible during testing.

The user interface proved intuitive. Push-button control of servo-driven fog rakes allowed precise manipulation of flow visualization, and the entire setup could be adjusted in less than five minutes between tests. Importantly, the modular design permitted individual component servicing without dismantling the entire system, enhancing the usability and educational value of the setup.

Overall, the complete system demonstrated its capability not only as a measurement tool but also as a teaching platform for aerodynamic principles. By combining direct force measurement with visible flow behavior, users could immediately correlate changes in design geometry with changes in aerodynamic performance.

5.4 Discussion of Limitations

While the system performed exceptionally well, several limitations were observed. The airflow velocity, although adequate for most automotive scale model testing, was limited to approximately 120 km/h due to fan capacity. Future iterations could benefit from variable-speed blowers or converging nozzle designs to increase test speeds and turbulence control.

Additionally, while the DFR system provides excellent qualitative feedback, it does not support quantitative flow visualization such as velocity vector mapping or vorticity plots. Integrating laser-based flow visualization (e.g., particle image velocimetry, PIV) in the future could enhance data depth for research applications.

Despite these constraints, the present system balances cost, complexity, and performance in a way that makes it accessible and highly functional for educational and experimental environments.

This section completes the analytical component of the paper. The experimental results and visual data collectively confirm the viability of the developed system for small-scale aerodynamic testing and iterative design evaluation. The wind tunnel's modularity, accuracy, and integration of both force and flow analysis tools present a compelling case for its broader adoption in university labs, motorsport startups, and R&D settings.

6. Conclusion

The objective of this research was to design, develop, and validate a low-cost, modular, and electronically controlled subsonic wind tunnel capable of measuring aerodynamic parameters and visualizing flow behavior around scaled automotive models. This objective was fully realized through the successful integration of core engineering domains—mechanical design, sensor interfacing, microcontroller programming, and aerodynamic analysis.

The developed system utilizes a strain gauge-based load cell and a Pitot tube-differential pressure sensor pair, integrated through an Arduino Uno microcontroller to provide real-time aerodynamic data such as downforce and airflow velocity. The control logic was structured to be modular, responsive, and user-friendly, allowing efficient calibration, consistent data acquisition, and intuitive feedback via an onboard LCD display. A notable achievement was the use of the HX711 24-bit analog-to-digital converter to amplify and digitize force data with high accuracy, enabling precise downforce measurements even in the sub-Newton range.

One of the most innovative components of this project is the Dynamic Flow Representation (DFR) system, a fog-based flow visualization mechanism designed to offer real-time, qualitative insight into airflow behavior. By integrating servo-controlled rakes and a commercially available fog generator, the system provides a compelling educational tool that visually demonstrates aerodynamic phenomena such as flow separation, boundary layer transition, and vortex formation. The ability to move fog vertically and horizontally enabled comprehensive flow interrogation across different sections of the test model.

Experimental validation was carried out using three distinctly shaped rear wing models—each representing a different aerodynamic strategy. The quantitative results from physical testing aligned closely with CFD simulations, confirming the accuracy of the developed measurement systems. The most efficient wing design, modeled after a Formula 1 configuration, achieved the highest downforce and lift-to-drag ratio, affirming both the aerodynamic fidelity of the wind tunnel and its applicability to real-world design evaluation.

The system also demonstrated strong operational reliability and ease of use. With its modular build, it supports rapid setup, reconfiguration, and maintenance. All components—mechanical, electronic, and software—were selected and assembled with a focus on replicability, making the entire setup highly suitable for educational laboratories, motorsport development teams, and entry-level R&D units.

Despite its success, the system does have certain limitations. The airflow speed is currently constrained by the fan assembly to approximately 120 km/h, which may limit its use in simulating high-speed highway or racing scenarios. Additionally, the fog-based visualization, while effective for qualitative interpretation, lacks the precision of advanced techniques like Particle Image Velocimetry (PIV) or Schlieren imaging. These limitations present opportunities for future improvements, including the integration of variable-speed fans, improved aerodynamic isolation, and advanced optical flow diagnostics.

In summary, this research has led to the creation of a robust, scalable, and functionally rich wind tunnel testing platform. It combines real-time quantitative measurement with qualitative flow visualization in a compact, affordable package. Its successful deployment and testing confirm its potential to democratize access to aerodynamic testing and education, bridging the gap between theoretical design and physical performance validation. The

system stands as a viable blueprint for institutions and independent researchers seeking a practical tool for studying vehicle aerodynamics

References

[1] B. Badamasi, "The working principle of an Arduino," *2014 11th International Conference on Electronics, Computer and Computation (ICECCO)*, Abuja, Nigeria, 2014, pp. 1–4. doi: 10.1109/ICECCO.2014.6997578.

[2] X. Wang, Y. Han, and S. Liu, "Design of a low-power environmental monitoring system using Arduino Uno and ZigBee," *Sensors & Transducers*, vol. 192, no. 9, pp. 45–50, Sep. 2015.

[3] A. Galadima, "Arduino as a learning tool," *International Journal of Engineering Research and Technology (IJERT)*, vol. 3, no. 2, pp. 1220–1224, Feb. 2014.

[4] D. Fransiska, M. Fatichah, and M. H. Purnomo, "Arduino and LabVIEW-based electrical power monitoring system," *International Conference on Intelligent Technology, System and Application (ITSA)*, 2015, pp. 130–134.

[5] N. Kumari, R. Yadav, and S. Dahiya, "An overview on Arduino board as the experimental tool for automation and control," *International Journal of Science, Engineering and Technology Research (IJSETR)*, vol. 5, no. 2, pp. 1655–1658, Feb. 2016.

[6] J. Müller, P. Huber, and A. Arndt, "Measurement of forces and torques using strain gauges and load cells," *Measurement Science and Technology*, vol. 22, no. 9, Sep. 2011. doi: 10.1088/0957-0233/22/9/092001.

[7] Y. H. Lee, J. H. Lee, Y. G. Yoon, J. W. Jeong, and Y. H. Cho, "High-sensitivity flexible strain sensor based on single-walled carbon nanotube film," *Sensors and Actuators A: Physical*, vol. 240, pp. 103–109, May 2016.

[8] A. Cho, J. Yoo, and H. Kim, "Wind estimation using Pitot tubes and GPS for small unmanned aerial vehicles," *Sensors*, vol. 15, no. 5, pp. 10639–10664, May 2015. doi: 10.3390/s150510639.

[9] M. Klopfenstein, "Air velocity measurement systems using Pitot tubes," *HVAC&R Research Journal*, vol. 11, no. 3, pp. 567–580, Jul. 2005.